Water Resources Research

RESEARCH ARTICLE
10.1029/2018WR022692

Cosmic Ray Neutron Sensing for Simultaneous Soil Water Content and Biomass Quantification in Drought Conditions

J. Jakobi[1], J. A. Huisman[1], H. Vereecken[1], B. Diekkrüger[2], and H. R. Bogena[1]

[1]Agrosphere Institute (IBG-3), Forschungszentrum Jülich, Jülich, Germany, [2]Department of Geography, University of Bonn, Bonn, Germany

Key Points:
- Soil water content and aboveground biomass were simultaneously and noninvasively measured using cosmic ray neutron sensing
- Cosmic ray neutron-based soil water content measurements were corrected for aboveground biomass using the thermal-to-fast neutron ratio
- Noninvasive biomass observations revealed the negative effects of drought conditions on sugar beet biomass development

Supporting Information:
- Supporting Information S1

Correspondence to:
J. Jakobi,
j.jakobi@fz-juelich.de

Citation:
Jakobi, J., Huisman, J. A., Vereecken, H., Diekkrüger, B., & Bogena, H. R. (2018). Cosmic ray neutron sensing for simultaneous soil water content and biomass quantification in drought conditions. *Water Resources Research*, *54*. https://doi.org/10.1029/2018WR022692

Received 1 FEB 2018
Accepted 18 JUL 2018
Accepted article online 27 JUL 2018

Abstract Understanding the feedback mechanisms between soil water content (SWC) and biomass production is important for sustainable resources management. Here we present a new method enabling simultaneous noninvasive measurements of SWC and biomass dynamics based on cosmic ray neutron sensing (CRNS). Recently, it was suggested that the neutron ratio (N_r) between thermal neutron (*TN*) and fast neutron (*FN*) intensity contains information on other hydrogen pools like vegetation, canopy interception, and snow. The aim of this study is to evaluate the accuracy of simultaneous measurements of SWC and biomass dynamics during agricultural drought conditions using CRNS probes. To this end, we instrumented an arable field cropped with sugar beet with CRNS probes and a wireless in situ SWC sensor network. Belowground and aboveground biomass were sampled in monthly intervals. We found a linear relationship between N_r and the aboveground biomass that allowed to continuously quantify the dry aboveground biomass development throughout the growing season with a root-mean-square error from 0.14 to 0.22 kg/m^2. This information was used together with measured belowground biomass to correct for the effect of biomass on SWC determination with CRNS probes, which increased the accuracy of the SWC estimates considerably as indicated by the decrease of the root-mean-square error from 0.046 to 0.013 cm^3/cm^3. We anticipate that future research on the N_r can further improve the accuracy of SWC and biomass estimates and extend the application of CRNS to include canopy interception, ponding water, and snow water equivalent estimation for both stationary and roving CRNS systems.

1. Introduction

Soil water content (SWC) is one of the key state variables in the soil-vegetation-atmosphere continuum due to its important role in the exchange of water and energy at the soil surface (Vereecken et al., 2015). A decade ago, cosmic ray neutron sensing (CRNS) was proposed as an attractive noninvasive and field-scale method for SWC estimation (Zreda et al., 2008) in a footprint of up to 15 ha with a maximum penetration depth of about 80 cm (Köhli et al., 2015). Since then, more than 200 stationary CRNS stations have been installed worldwide (Andreasen, Jensen, Desilets, Franz, et al., 2017). A range of studies have successfully compared SWC estimates obtained with CRNS to in situ measurements (Baatz et al., 2014, 2015; Bogena et al., 2013, 2015; Franz, Zreda, Ferré, et al., 2012; Rivera Villarreyes et al., 2011; Schrön et al., 2017) and satellite and modeling products (Baatz et al., 2017; Kędzior & Zawadzki, 2016; Montzka et al., 2017; Vinodkumar et al., 2017). Clearly, CRNS has matured into an established noninvasive method for SWC determination that allows to bridge the gap between spaceborne and in situ (point-scale) SWC measurements (Bogena et al., 2015).

CRNS measurements are not only sensitive to SWC but are also influenced by hydrogen stored in other pools (Desilets et al., 2010), such as biomass, litter, snow, and canopy interception (Andreasen, Jensen, Desilets, Zreda, et al., 2017; Bogena et al., 2013; Schattan et al., 2017). To improve the accuracy of SWC estimates, these pools need to be considered. Static hydrogen pools such as soil organic carbon (Franz, Zreda, Rosolem, & Ferré, 2013) and lattice water (Franz, Zreda, Rosolem, & Ferré, 2012) can be accounted for with relatively small effort during the calibration of the CRNS probe. Time-varying hydrogen pools such as atmospheric water vapor content (Rosolem et al., 2013), vegetation biomass (Baroni & Oswald, 2015; Rivera Villarreyes et al., 2011), or the water content of a litter layer (Bogena et al., 2013) can be considered using independent estimates of these confounding variables. Whereas the influence of atmospheric water vapor content on the CRNS measurements can be accurately removed using measurements of air humidity (Rosolem et al., 2013), corrections for dynamic changes in biomass (e.g.,

growing crops) are much less straightforward because accurate field-scale estimates of biomass are laborious to obtain.

Recently, Tian et al. (2016) proposed to use the ratio of thermal to fast neutron intensity measured with the CRNS probe to estimate aboveground biomass for maize and soybean crops. Obviously, it would be highly attractive to estimate biomass directly using CRNS for at least two reasons. First, it would allow to remove effects of time-varying biomass from SWC estimates obtained with CRNS without the need for additional measurements. Several studies have already reported that biomass and the N_0 parameter (the fast neutron count rate over dry soil conditions) of the standard calibration model for CRNS probes are linearly or nonlinearly related (Baatz et al., 2014, 2015; Franz, Zreda, Rosolem, Hornbuckle, et al., 2013; Hawdon et al., 2014; Hornbuckle et al., 2012). In all these studies, the use of the proposed correction methods resulted in a considerable improvement in the accuracy of SWC estimates for sites with constant biomass (e.g., forests) or sites with near-constant biomass (e.g., deciduous forests; Heidbüchel et al., 2016). However, strong deviations were still found for cropped sites with dynamic changes in aboveground and belowground biomass. Clearly, a general method for the correction of biomass effects on CRNS measurements of SWC covering various vegetation types is still not available.

Second, simultaneous measurements of SWC and biomass dynamics at the field scale would be very useful to improve the understanding of relationships between plant growth and SWC deficit, which is essential for the development of adaptation strategies against drought-induced restrictions in crop production. According to Dai (2011), the risk for droughts has increased substantially since the 1970s due to global climate change (e.g., increased atmospheric moisture demand and altered atmospheric circulation patterns). The drought frequency has also increased in temperate climates since the 1980s (Briffa et al., 2009). Although this typically has not yet affected food security as in Sub-Saharan Africa (Webber et al., 2014), the economic losses due to drought have also been considerable in temperate climate regions. For example, the average cost of a drought event in Europe was estimated to be 621 million euros between 1950 and 2014 (Zink et al., 2016). Thus, securing and improving productivity of crops in water-limited conditions has become more important in recent years (Passioura & Angus, 2010).

The overall aim of this study is to evaluate the accuracy of simultaneous measurements of SWC and biomass dynamics using CRNS probes and to show the potential of CRNS measurements for identifying and studying effects of agricultural droughts on both soil water storage and plant growth. For this, we first evaluate available approaches to correct SWC estimates obtained from CRNS for biomass for the case of a highly dynamic crop with high belowground biomass. In a next step, we test the potential of simultaneous measurements of SWC and biomass dynamics using information of calibrated CRNS data only. For this study, we rely on data from an extensive field experiment where cosmic ray neutrons, biomass, and SWC were monitored in an agricultural field site cropped with sugar beet (*Beta vulgaris* L.) for an entire growing season.

2. Materials and Methods

2.1. The Selhausen Experimental Site

The Selhausen experimental site is part of the TERENO (TERrestrial ENvironmental Observatories) network (Bogena et al., 2012; Zacharias et al., 2011) and is located in Western Germany, 40 km west of Cologne (50°52′00″N 6°27′22″E). In this study, we focus on the F01 field at the Selhausen site that covers an area of 2.77 ha (Bogena et al., 2018). The site is located in the temperate maritime climate zone with a mean annual temperature and precipitation of 10.2 °C and 714 mm, respectively (Korres et al., 2015). The soil was classified as a Cambisol with a silty loam soil texture. The investigated field is located on the upper terrace of the Rhine/Meuse river system and is characterized by Pleistocene sand and gravel sediments (Weihermüller et al., 2007) with irregularly alternating subsurface channels that are filled with fine sediments. The within-field variability of soil properties was determined by Rudolph et al. (2015) using z-transformed electrical conductivity (σ_z) measurements (Figure 1). Lower values indicate a higher content of sand and gravel and thus a lower water-holding capacity, whereas higher σ_z values indicate finer material with higher water holding capacity. This heterogeneous sediment distribution leads to spatially variable plant development and leaf area index patterns (Rudolph et al., 2015).

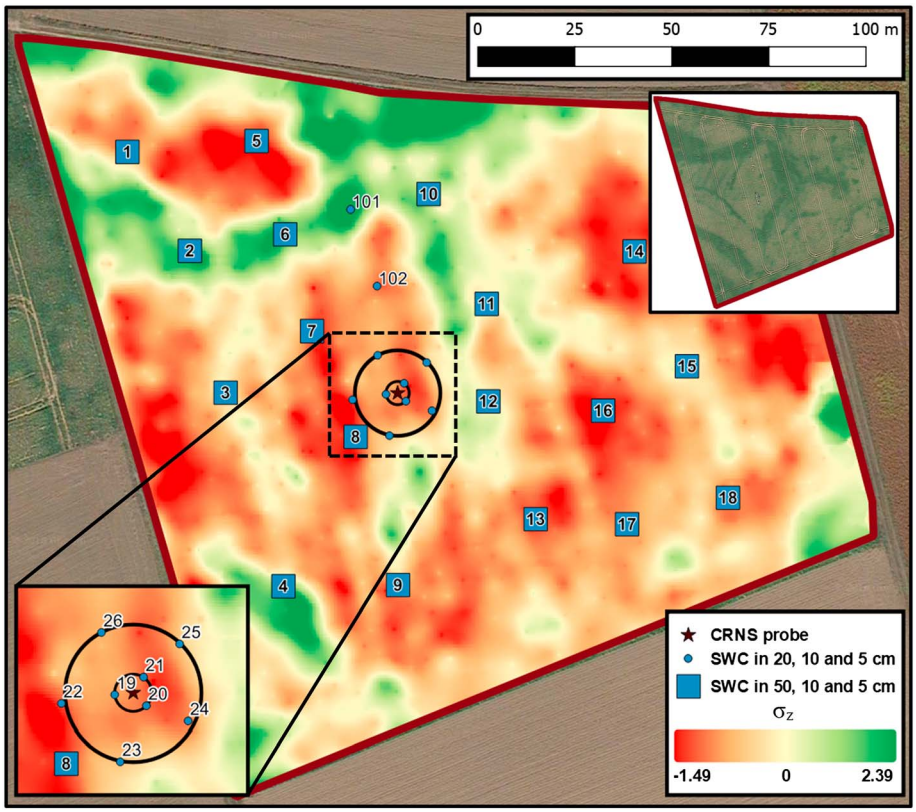

Figure 1. Map of the Selhausen experimental field showing z-transformed electromagnetic conductivity (σ_z) distribution and the locations of sampling and instruments. The σ_z measurements indicate gravel- and sand-dominated soils (reddish colors) with lower field capacity and fine material fillings (greenish colors) with higher field capacity (Rudolph et al., 2015). In the upper right corner, the google maps satellite image from the beginning of the dry period (9 August 2016) is shown. The pattern of healthier (dark green) and less healthy (light green) crops mirrors the distribution of σ_z values. CRNS = cosmic ray neutron sensing; SWC = soil water content.

2.2. Auxiliary Data

Air temperature, wind speed, absolute humidity, net radiation, and atmospheric pressure were measured during the experiment. The potential grass reference evapotranspiration (ET_{pot}) was calculated from the meteorological data using the Penman-Monteith equation according to Allen et al. (1998). Actual evapotranspiration (ET_{act}) was measured with an eddy covariance flux tower at approximately 5 m distance from the CRNS station following methods described in Gebler et al. (2015). Finally, we used precipitation data from a TERENO meteorological station approximately 500 m northwest of the Selhausen test site (SE_EC_003, http://teodoor.icg.kfa-juelich.de/ibg3searchportal2/index.jsp).

Several drought indices have been developed to assess and respond to drought based on various hydrological and meteorological parameters, including precipitation, evapotranspiration, and SWC (Narasimhan & Srinivasan, 2005). Here we use the evaporative index (potential evapotranspiration divided by precipitation), the water balance, and data from the German drought monitor (Zink et al., 2016) to characterize the drought situation during the investigation period. The German drought monitor is based on a soil moisture index that considers the modeled average profile SWC of the past 30 days and the average modeled profile SWC for the selected time period for the past 60 years (Zink et al., 2016).

2.3. In Situ SWC Measurements

In situ SWC was measured at each of the sampling sites (1–26, Figure 1) in three depths with the SoilNet wireless sensor network (Bogena et al., 2010) equipped with 156 SMT100 SWC sensors (Truebner GmbH, Neustadt, Germany). Two SMT100 sensors were installed per sampling depth to increase the measurement volume and to enable the identification of sensor malfunctioning. The SMT100 sensors were

Figure 2. Setup of the cosmic ray neutron sensing probes at the test site Selhausen (three CRS-2000/B [1, 2, and 3], one CRS-1000 [4], and one CRS-cross calibrator [5]).

individually calibrated using five dielectric reference media (Bogena et al., 2017), and the measured permittivity was related to SWC using the Topp equation (Topp et al., 1980). We considered the soil heterogeneity for the selection of locations 1–18 (Figure 1) for soil sampling (section 2.6) and the in situ SWC measurements. Additional locations were selected near the CRNS probe to consider the greater sensitivity of the detector to neutrons originating closer to the sensor (Köhli et al., 2015; Schrön et al., 2017). Therefore, eight additional locations were positioned radially around the CRNS probes at a distance of 3 m (locations 19–21) and 11 m (locations 22–26). The SMT100 sensors at locations 1–18 were installed in 5-, 20-, and 50-cm depths. At locations 19–26, the sensors were installed in 5-, 10-, and 20-cm depths. This was done to favor a higher resolution close to the soil surface and to also account better for the decreasing sensitivity of the CRNS probes with soil depth (Zreda et al., 2008).

In order to compare CRNS probe and in situ SWC measurements, it is necessary to integrate the distributed SoilNet measurements considering the spatial sensitivity of the CRNS probes. We followed the averaging procedure developed by Köhli et al. (2015) and Schrön et al. (2017), which provides an improved estimate of the spatial sensitivity of the CRNS probe as compared to the simple exponential decay initially suggested by Zreda et al. (2008). The neutron transport simulation used to derive this revised spatial sensitivity also showed that the sensitivity with depth decreases exponentially and not linearly as assumed by Franz, Zreda, Ferré, Rosolem, et al. (2012). A detailed description of the averaging of the distributed SWC measurements used for comparison with CRNS measurements is given in Appendix A.

2.4. Determination of Biomass Dynamics

We sampled sugar beet biomass at nine locations (Figure 1, locations 22–26, 2, 16, 101, and 102) on a monthly basis. The selection of locations 22–26 close to the CRNS probes was based on the assumption that hydrogen sources at shorter distance have a greater influence on the CRNS signal. Some additional biomass sampling locations were used to represent both favorable (locations 2 and 101) and less favorable growing conditions (locations 16 and 102). We used the arithmetic mean of all biomass sampling locations as the best representative estimate of the biomass sensed by the CRNS probe. At each biomass sampling location, 1 m of planting row was harvested. This included both aboveground and belowground biomass down to a depth of ~40 cm, which corresponds to the maximum penetration depth of the CRNS probe for the lowest SWC measured during the measurement period. Areal average biomass was calculated from the average distance between rows (46.5 cm). The biomass samples were bagged and sealed airtight before they were transported to the laboratory. In the laboratory, they were cleaned from soil residues, divided into aboveground and belowground biomass, and weighed. In order to determine dry biomass, subsamples of ~20% of the biomass were oven dried to a constant weight at 65 °C. The vegetation water content was estimated from the weight loss after drying. Total biomass water equivalent (BWE) consists of vegetation water as well as hydrogen present in the biomass tissue. As suggested by Franz, Zreda, Rosolem, and Ferré (2013) and Franz, Zreda, Rosolem, Hornbuckle, et al. (2013), we assume that the water equivalent of the aboveground and belowground biomass can be approximated by the amount of hydrogen and oxygen contained in cellulose (f_{ew}), that is, ~55.6% by weight:

$$BWE = [(BM_f - BM_d) + f_{ew} \cdot BM_d] \cdot \rho_w \cdot p_d \quad (1)$$

where p_d is the plant density (plants m^{-2}), BM_f and BM_d are fresh and dry biomass weights (kilograms), respectively, and ρ_w is the density of water (10^3 kg/m^3). This equation was used for the determination of

aboveground BWE (BWE_a), belowground BWE (BWE_b), and total BWE ($BWE_{tot} = BWE_a + BWE_b$). Between sampling dates, estimates of BWE were obtained by linear interpolation.

2.5. Cosmic Ray Neutron Measurements

We used five CRNS probes (one CRS-1000, three CRS-2000/B, and one mobile CRNS probe, Figure 2), each equipped with two detector tubes. Summing up the measured neutron counts from all systems resulted in a much higher neutron intensity accuracy compared to a single probe. All probes were manufactured by Hydroinnova LLC, Albuquerque, NM, United States. The neutron detectors are either filled with ^{3}He gas (CRS-1000 and mobile CRNS probe) or $^{10}BF_3$ (CRS 2000/B) enriched gas to obtain high neutron absorption cross sections. When neutrons enter the detector tube, the gases absorb part of the neutrons, which creates electrons that are attracted by an anode. This produces electric currents which are amplified, detected, and counted by a pulse module (Zreda et al., 2012). The neutron absorption of ^{3}He is more efficient, and thus these detector tubes can be constructed distinctly smaller compared to $^{10}BF_3$-filled detector tubes. For this reason, ^{3}He detector tubes are installed inside protective housings (Figure 2, tube 4 and CRS-cross calibrator — no. 5), whereas the larger $^{10}BF_3$-filled detector tubes are mounted on poles without a housing (Figure 2, tubes 1–3).

Cosmic ray neutrons can be differentiated into two energetic levels (Köhli et al., 2015): thermal neutrons (*TN*, maximum energy at ~0.025 eV) and fast neutrons (*FN*, energy range from ~0.2 eV to 100 keV). *FN* are continuously losing energy by collisions with atomic nuclei and other neutrons, a process called moderation, and will eventually be transformed into *TN*. Because of the lower kinetic energy, the probability of absorption reactions is greater for *TN*. Unshielded detector tubes respond mainly to neutrons in the thermal energy range. To detect neutrons in the fast energy range, the detector tube is shielded with polyethylene, which has a high hydrogen content that effectively moderates *FN* to *TN* before they enter the detector tube.

It is well established that *FN* are subject to variations in air pressure (Desilets & Zreda, 2003), incoming cosmic ray neutron intensity (Desilets & Zreda, 2001), and atmospheric water vapor (Rosolem et al., 2013). We applied the established correction methods for all three influences to obtain corrected *FN* intensity data (see Appendix B). However, the required corrections for *TN* intensity are still under debate. For instance, Tian et al. (2016) used uncorrected *TN* intensity to estimate the thermal-to-fast neutron ratio, *Nr* (see section 2.7), whereas Andreasen, Jensen, Desilets, Zreda, et al. (2017) corrected *TN* intensity for air pressure and incoming neutron variations. In order to investigate the most appropriate correction procedure, we empirically explored various *TN* correction procedures (Appendix C). We found that the best results were achieved with *TN* intensity corrected for pressure and atmospheric water vapor only. This suggests that *TN* intensity is less dependent on incoming cosmic radiation than *FN* intensity. At first sight, this may seem surprising as *TN* are typically produced by thermalization of *FN*. However, absorption (e.g., by Gd, Ti, and B) and diffusion processes become more important in the *TN* energy range (Schrön, 2017; Zreda et al., 2008), which is expected to weaken the relationship between *FN* and *TN*. More elaborated studies using neutron transport modeling are needed to better address the determination of the most appropriate correction strategy for *TN* intensity.

2.6. Static Belowground Hydrogen Pools

The CRNS method is affected by all hydrogen pools, which may be divided into desired signals, such as SWC and vegetation biomass, and distorting influences, such as soil organic matter and lattice water (Zreda et al., 2012). The distorting belowground hydrogen pools decrease the neutron count and reduce the effective sensing depth of CRNS probes (Bogena et al., 2013; Franz, Zreda, Rosolem, & Ferré, 2012). In this study, soil organic matter, lattice water (*LW*), and soil bulk density were determined using soil cores of 30-cm length and 5-cm diameter taken at locations 1–26 (Figure 1) with a HUMAX soil corer (Martin Burch AG, Rothenburg, Switzerland). The soil cores were divided into 5-cm-long subsamples, and their bulk density was derived using the oven drying method (105 °C, 24 hr). Subsequently, these 156 samples were sieved and merged to six depth-specific bulk samples of which 20-mg subsamples were combusted in oxygen at 1000 °C in order to determine *LW* using a heat conductivity detector. The total organic carbon (*TOC* [g/g]) of the bulk subsamples was determined using a VARIO EL Cube (Elementar Analysensysteme GmbH,

Langenselbold, Germany). The soil organic carbon water content equivalent (*SOW* [g/g]) was estimated according to Franz et al. (2015):

$$SOW = TOC \cdot 1.724 \cdot f_{ew} \tag{2}$$

where the constant 1.724 is used to convert total organic carbon mass into soil organic matter mass, and f_{ew} is the stoichiometric ratio of water to cellulose ($C_6H_{12}O_5$, i.e., ~55.6% of the dry weight). It was found that the *LW* content averaged over space and depth was 0.0289 ± 0.006 g/g. *SOW* averaged over all locations and depths was 0.01 ± 0.0025 g/g. The minimum bulk density of 1.2 g/cm^3 was measured at location 13, the average bulk density was 1.36 g/cm^3, and the maximum bulk density of 1.46 g/cm^3 was measured at location 10.

2.7. Thermal-to-Fast Neutron Ratio

Tian et al. (2016) found that the ratio of thermal to fast neutron counts (N_r) was positively correlated with BWE_a for maize and soybean crops and thus could be used to estimate biomass. This finding was recently confirmed using neutron modeling for agricultural, heathland, and forest sites by Andreasen, Jensen, Desilets, Zreda, et al. (2017). In this study, we used the following definition of the N_r:

$$N_r = \frac{TN \cdot \frac{FN_{av}}{TN_{av}}}{FN} \tag{3}$$

where *FN* and *TN* intensity were integrated using a 3-day moving average and FN_{av} and TN_{av} were the arithmetic means for the entire measurement period. The 3-day integration time was chosen to reduce the effect of highly dynamic hydrogen pools (i.e., interception, ponding water, and infiltration fronts succeeding precipitation), which are associated with relatively short time scales (i.e., less than a day). In contrast, biomass changes occur much slower (i.e., time scale of days to weeks; Baroni & Oswald, 2015). The normalization was introduced to enable a better comparison with other studies using different numbers of detector tubes. Following Tian et al. (2016), we related BWE_a to N_r using a linear model:

$$N_r - BWE_a = a \cdot N_r + b \tag{4}$$

where a and b are calibration parameters and N_r-BWE_a represents BWE_a calculated from the N_r. Since dry aboveground biomass (AGB_d) instead of BWE_a is used in most agricultural management and environmental modeling applications, we also examined whether this property can be estimated from N_r-BWE_a. For this, equation (1) was reformulated (see Appendix D):

$$N_r - AGB_d = \frac{N_r - BWE_a}{\left(\frac{1}{AGB_r} + f_{ew} - 1\right)} \cdot \frac{1}{p_w \cdot p_d} \tag{5}$$

where N_r-AGB_d is the dry aboveground biomass calculated from the N_r and the measured ratio (AGB_r) of AGB_d to fresh aboveground biomass (AGB_f), which was calculated with

$$AGB_r = \frac{AGB_d}{AGB_f} \tag{6}$$

In typical applications, only a single value for AGB_r (i.e., the average of AGB_r over the growing season) may be available. Therefore, we also tested whether an adequate estimation of AGB_d is possible using a constant AGB_r.

2.8. Relating Fast Neutron Intensity to SWC and Accounting for Biomass

Baatz et al. (2014) compared three parametrization methods to infer SWC from *FN* intensity and found that all methods performed reasonably well (root-mean-square error [RMSE] ≤0.033 cm^3/cm^3). We chose the N_0 method (Desilets et al., 2010) as it has been successfully applied in various studies (e.g., Baatz et al., 2014, 2015; Baroni & Oswald, 2015; Bogena et al., 2013; Franz, Zreda, Ferré, et al., 2012; Franz, Zreda, Rosolem, &

Table 1
Summary of Correction and Calibration Methods Used in This Study, as Well as Respective RMSE Values, Data Requirements, and Involved Equations and Figures

Biomass correction	Calibration methods	RMSE cm^3/cm^3	Data requirements	Equation	Figure
Not considered	Method 1: Standard CRNS calibration (e.g., Zreda et al., 2012)	0.125	One-time representative in situ SWC estimate in the CRNS footprint (SWC_{if})	(7)	4
	Method 2: CRNS calibration using SWC time series (e.g., Bogena et al., 2013)	0.046	Continuous SWC_{if}	(7)	4
Aboveground biomass	Method 3a: biomass correction according to Baatz et al. (2015)	0.095	One SWC_{if}, BWE_a	(7)	5 and 13
	Method 3b: standard biomass correction calibrated using in situ data	0.036	Multiple SWC_{if}, BWE_a	(7) and (8)	5, 6 and 13
	Method 3c: N_r biomass correction	0.032	Multiple SWC_{if} (here continuous), *TN*	(7) and (10)	12 and 13
Total biomass	Method 3d: standard biomass correction calibrated using in situ data	0.019	Multiple SWC_{if}, BWE_{tot}	(7) and (9)	5, 6 and 11
	Method 3e: combined in situ BWE_b and N_r biomass correction	0.013	Multiple SWC_{if}, BWE_{tot}, *TN*	(7) and (9)	10 and 11

Note. RMSE = root-mean-square error; CRNS = cosmic ray neutron sensing; SWC = soil water content.

Ferré, 2012; Franz, Zreda, Rosolem, Hornbuckle, et al., 2013; Franz et al., 2015; Rivera Villarreyes et al., 2011; Tian et al., 2016):

$$\theta_v(t) = p_{bd}\left[a_0\left(\frac{FN(t)}{N_0(t)} - a_1\right)^{-1} - a_2 - LW - SOW\right] \tag{7}$$

where θ_v is the volumetric SWC (cm^3/cm^3), N_0 is the fast neutron count rate over dry soil, t indicates the time dependency, ρ_{bd} is the average dry soil bulk density of all locations (g/cm^3), and a_i are fitting parameters. Using MCNPx simulations for generic silica soils, Desilets et al. (2010) derived $a_0 = 0.0808$, $a_1 = 0.372$, and $a_2 = 0.115$ for values of $\theta > 0.02$ kg/kg. In this study, a 12-hr moving average of *FN* intensity was used for SWC estimation.

Local calibration of the CRNS probes was done by fitting N_0 in equation (7) to in situ SWC measurements. We used three calibration methods: Method 1 calibration of N_0 at one specific day (e.g., Desilets et al., 2010), Method 2 calibration of N_0 using the continuously measured SWC and *FN* during the monitoring period (e.g., Bogena et al., 2013), and Method 3 calibration of N_0 at one specific day complemented with correction procedures to account for the impact of biomass on the measured *FN* intensity (e.g., Baatz et al., 2015). Methods 1 and 2 are used to illustrate the need for biomass correction of CRNS data. The correction functions required for the third approach were obtained by relating time-variable N_0 estimates derived from *FN* intensity and reference SWC with a range of quantities that represent the vegetation influence on *FN*. In particular, the following linear regression functions were considered:

$$N_{0,BWEa}(t) = c_{BWEa} \cdot BWEa(t) + N_{0,BWEa=0} \tag{8}$$

where c_{BWEa} in counts per hour (cph) per millimeter of BWE_a represents the change in N_0 with BWE_a and $N_{0,BWEa=0}$ is the intercept of the regression

$$N_{0,BWEtot}(t) = c_{BWEtot} \cdot BWE_{tot}(t) + N_{0,BWEtot=0} \tag{9}$$

where c_{BWEtot} in counts per hour (cph) per millimeter of BWE_{tot} represents the change in N_0 with BWE_{tot} and $N_{0,BWEtot=0}$ is the intercept of the regression, and

$$N_{0,N_r}(t) = c_{N_r} \cdot N_r(t) + N_{0,N_r=0} \tag{10}$$

where c_{Nr} in counts per hour (cph) per one N_r (the N_r is given in arbitrary units; see section 2.7) represents the change in N_0 with the N_r, and $N_{0,Nr=0}$ is the intercept of the regression. The different calibration variants used in this study are summarized in Table 1.

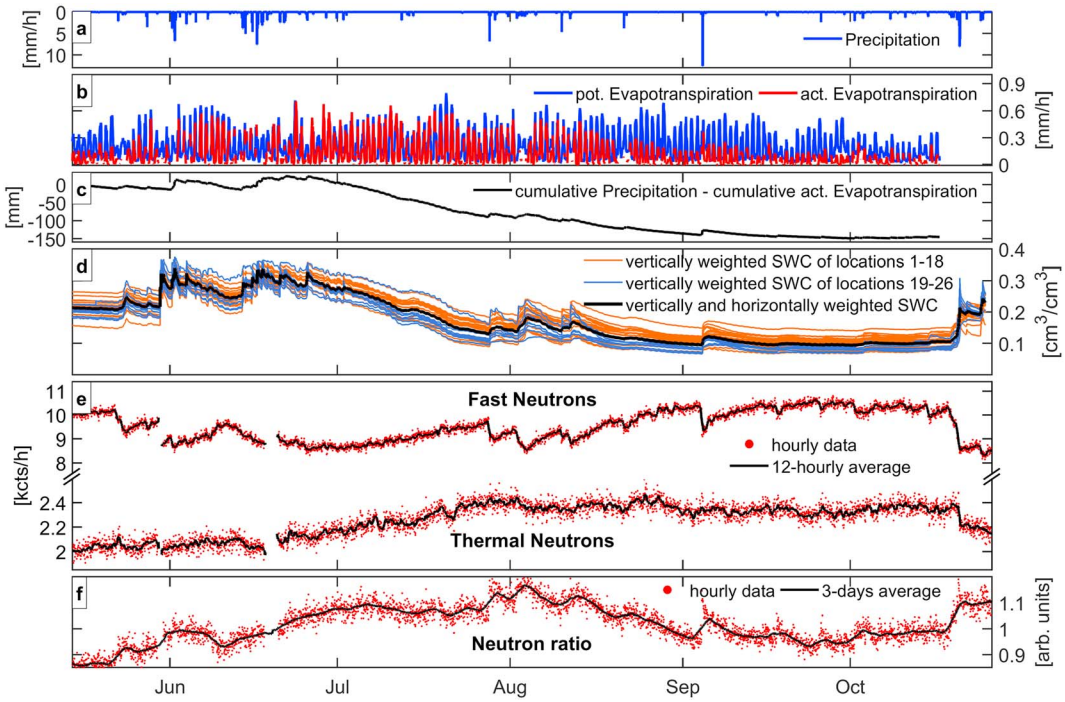

Figure 3. Time series of (a) precipitation, (b) potential and actual evapotranspiration, (c) the water balance (cumulative precipitation minus cumulative actual evapotranspiration, runoff is negligible as the site has almost no inclination), (d) SWC, (e) *FN* and *TN* intensity, and (f) neutron ratio, N_r. For SWC, the vertically and horizontally weighted SWC using all SWC measurements (black line) and the vertically weighted SWC of the 26 SoilNet locations is shown. Please note that at locations 1–18 SWC was measured in 5-, 20-, and 50-cm depths (orange lines), whereas at locations 19–26 SWC was measured in 5-, 10-, and 20-cm depths (blue lines). Locations 19–26 exhibit lower σ_z values and thus water holding capacities which resulted in lower SWC. SWC = soil water content.

3. Results

3.1. CRNS Measurements

The continuously measured *FN* and *TN* intensity at the Selhausen site during the growing season is presented in Figure 3e. On average, the count rate of *FN* was about 5 times higher than the *TN* count rate (maximum, mean, and minimum count rates per hour for *FN* and *TN* were 10,801, 9,484, 8,148, and 2,588, 2,212, 1,820, respectively). This is partly related to the measurement setup with different amount of detectors for *FN* and *TN* (three *TN* vs. seven *FN* detectors). In a drying period after frequent precipitation in June, a clear increasing trend in *FN* and *TN* intensity can be observed. This is because of the progressing decrease in SWC due to low precipitation and increasing evaporative demand, which can also be observed in the water balance for the measurement period (accumulated precipitation minus accumulated actual evapotranspiration, Figure 3c). Sharp decreases in *FN* (and to a lesser degree in *TN*) are related to strong precipitation events and the associated increases in SWC. These are particularly evident at the end of October where the evaporative demand has already decreased strongly.

3.2. In Situ SWC Measurements

The general course of vertically weighted SWC time series derived from the in situ SWC measurements mirrors the results from the neutron count measurements (Figure 3d). However, relatively strong differences in absolute SWC are also visible between the sampling locations throughout the measurement period. After July, the vertically weighted SWC at locations 19–26, which are closer to the CRNS probes, was generally lower than SWC at the locations further away. An exception is the higher SWC at location 25, which was related to a tractor track with highly compacted soil and low plant density that reduced both infiltration and water extraction by vegetation at this particular location. Although the in situ measurements at stations 19–26 are restricted to the first 20 cm, the vertically weighted SWC data from these stations fall within the overall observed SWC range. Thus, we conclude that the in situ SWC data from the SoilNet stations capture the heterogeneous soil properties within the test field.

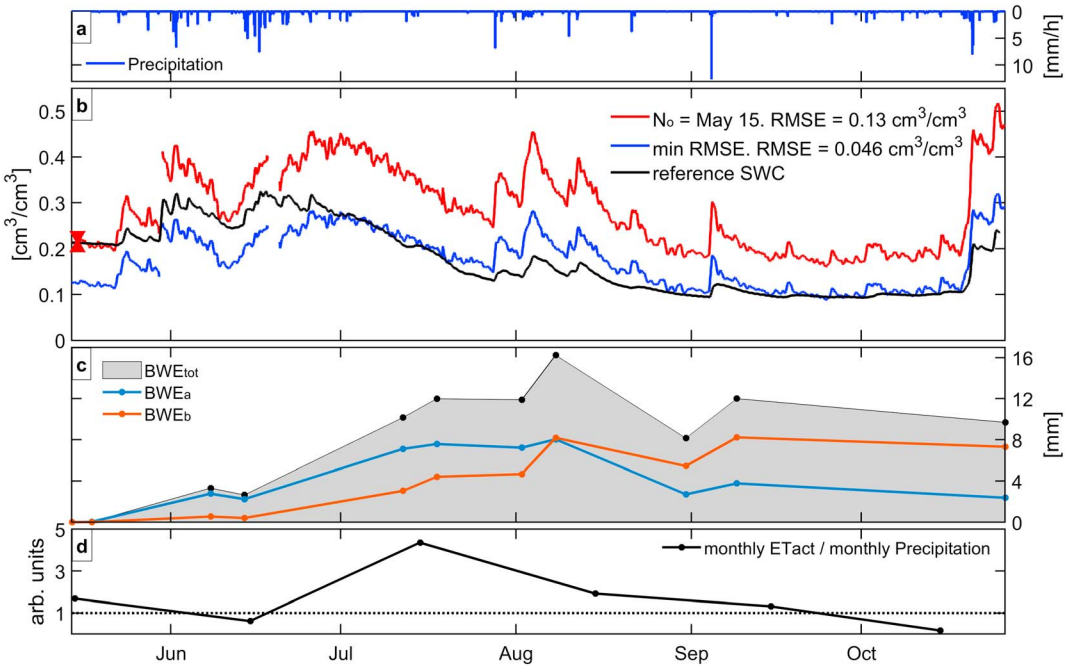

Figure 4. Time series of (a) precipitation, (b) soil moisture derived from *FN* intensity measurements and in situ SoilNet sensors, (c) measured and interpolated biomass development from May to October 2016, and (d) the development of the ratio of monthly actual evapotranspiration and monthly precipitation. For soil moisture estimation, the cosmic ray neutron sensing probe was either calibrated using only one day (15 May, red arrows) before the biomass development started (Method 1, red line) or using the whole time series of in situ soil moisture (Method 2, blue line). RMSE = root-mean-square error.

3.3. Biomass Development

The measured development of BWE_{tot} as well as BWE_a and BWE_b are shown in Figure 4c. All three biomass measures increase until the end of July, and BWE_a makes up the largest proportion of BWE_{tot}. However, BWE_a started to decline noticeably in August, which coincides with a 2-month-long period of very low SWC (Figure 3d). During this period, the actual evapotranspiration was also substantially lower than the potential evapotranspiration (Figure 3b), indicating a prolonged drought situation that led to the drying of leafs and leaf loss of the sugar beet plants. The spatially variable health status of the plants can also be observed on a satellite image from 9 August 2016 (Figure 1, top right), and the German drought monitor indicated that the study region experienced a moderate to severe drought during September and October. Such droughts typically occur every 3–6 years and likely result in damage to crops and pasture (Zink et al., 2016). The drought period was initiated in July where the cumulative actual evapotranspiration exceeded precipitation by a factor of 4 (Figure 4d). Interestingly, the development of belowground biomass was less affected by the summer drought as BWE_b remained fairly constant after early August and increased strongly in the beginning of September. The drought-induced decrease of BWE_a and the stagnation of belowground biomass growth led to a strong decrease in BWE_{tot} during August. These findings demonstrate that the growth of sugar beets at our test site was strongly influenced by water availability and that aboveground and belowground biomass development were influenced by drought to a different extent.

3.4. SWC Estimation Without Biomass Correction

Figure 4b shows the result of two different calibration approaches, both without the consideration of dynamic changes in biomass. In Method 1, we used the in situ SWC from 15 May for calibration (red arrows, Figure 4b). At this time, the field was free of vegetation. This method represents a calibration strategy used in many CRNS studies (i.e., a single calibration at or shortly after detector deployment). The SWC estimates obtained using this single calibration showed a growing discrepancy with the reference SWC estimates throughout the measurement period, and the resulting RMSE of ~0.13 cm^3/cm^3 is high. In Method 2, the whole time series of in situ SWC measurements was used for the calibration of a single value of N_0. It can be observed that the SWC estimates derived from CRNS measurements using this method also clearly

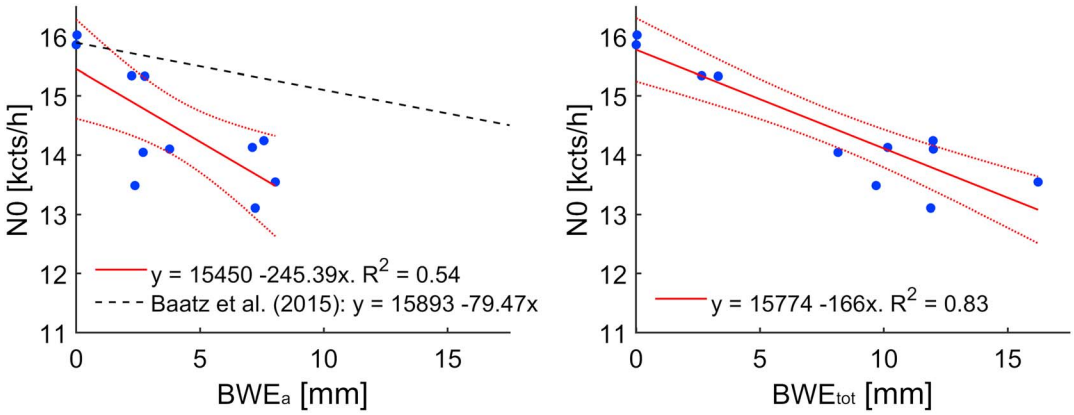

Figure 5. Relationship between N_0, calibrated at the times of biomass measurements using equation (7), and BWE_a and BWE_{tot}. The left plot also shows the linear regression function proposed by Baatz et al. (2015), which shows a considerably flatter slope.

deviate from the reference SWC. In particular, SWC is underestimated until July and overestimated after July. However, the resulting (RMSE) of 0.046 cm^3/cm^3 is still reasonably close to previous studies, for example, ~0.039 cm^3/cm^3 in Rivera Villarreyes et al. (2011) and 0.033 cm^3/cm^3 in Baatz et al. (2014). These results clearly show that a single value of N_0 cannot be used to accurately predict SWC, which we attribute to a strong influence of biomass on the *FN* intensity.

3.5. SWC Estimation With Biomass Correction Using In Situ Measurements

First, we determined the calibration parameter N_0 for each biomass sampling date from the measured FN intensity and the reference SWC and correlated it with measured BWE_a and BWE_{tot} (Figure 5). The empirical correction function of Baatz et al. (2015) has a considerably flatter slope in comparison to the site-specific regression function (Figure 5, left). This indicates that site-specific calibration may be preferable for cropped fields with relatively low biomass (i.e., dry aboveground biomass less than 5 kg/m^2) as the correction function of Baatz et al. (2015) was developed using data from forest sites with much higher amounts of biomass. The linear regression between BWE_{tot} and N_0 provided a higher correlation coefficient compared to the linear regression between BWE_a and N_0 (R^2 = 0.83 vs. 0.54). Using these linear relationships and interpolated BWE_a and BWE_{tot} estimates (Figure 4c), a temporally variable N_0 was estimated and used to derive SWC estimates corrected for dynamic changes in biomass with equations (7) and (8) (i.e., BWE_a correction) or equation (9) (i.e., BWE_{tot} correction). The accuracy of the SWC estimates as expressed by the RMSE improved to 0.036 cm^3/cm^3 when the temporally variable N_0 was estimated from BWE_a and to 0.019 cm^3/cm^3 when N_0 was estimated from BWE_{tot} (Figure 6).

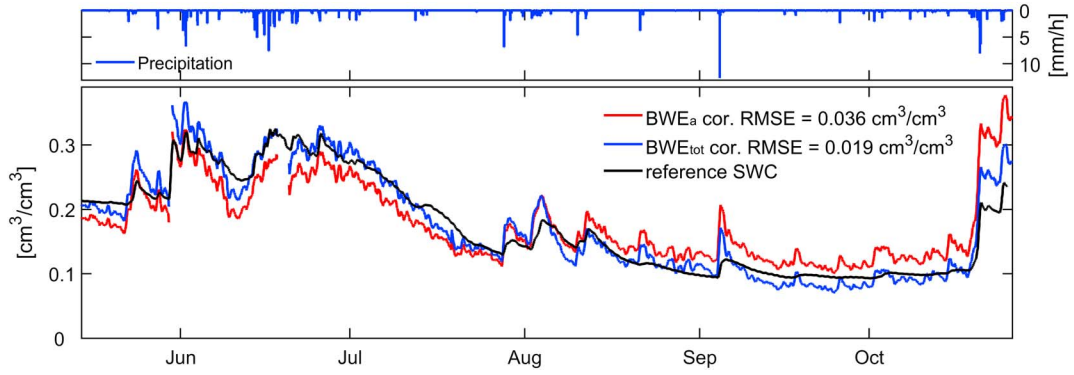

Figure 6. Reference in situ SWC (black line) and *FN*-derived SWC estimates corrected using equations (7) and (8) with BWE_a (Method 3b, red line) and equations (7) and (9) with BWE_{tot} (Method 3d, blue line). SWC = soil water content; RMSE = root-mean-square error.

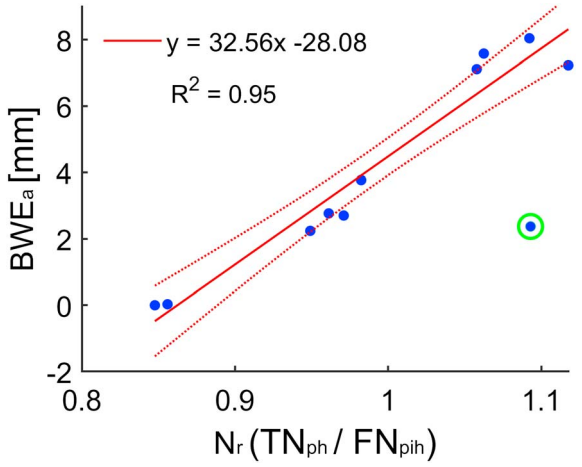

Figure 7. Relationship between BWE_a and the N_r. The outlier marked in green coincided with an extensive precipitation event at the end of the measurement period and was therefore removed from the analysis.

SWC corrected using BWE_a underestimated the reference SWC until the beginning of August, while SWC was overestimated for the remaining period (Figure 6). We attribute this to the variable ratio between aboveground and belowground biomass of sugar beet (Figure 4c), which was not considered in the correction using BWE_a. Therefore, we anticipate that BWE_a measurements may be sufficient for the correction of CRNS-derived SWC in the case of vegetation with a relatively constant root-to-shoot ratio (i.e., BWE_b to BWE_a ratio). For the more common case where this ratio is dynamic, a correction considering both BWE_a and BWE_b (i.e., BWE_{tot}) will improve the accuracy of CRNS-derived SWC.

When BWE_{tot} is used for correction, notable deviations between estimated and reference SWC still occur during and several days after precipitation events (e.g., in the beginning of August and September, as well as in the last week of the measurement period). This may be due to other hydrogen pools currently not accounted for, such as interception and ponding water, or shallow wetting of the soil surface not captured by the in situ SWC sensors.

3.6. BWE_a Estimation From the Neutron Ratio

Figure 7 shows the linear relationship between measured BWE_a and the neutron ratio, N_r, determined from the *FN* and *TN* intensity at the biomass sampling days. One obvious outlier, which corresponds to the last biomass measurement, was excluded from the regression analysis (Figure 7, marked in green) because the neutron signal was probably influenced by other hydrogen pools (e.g., interception and ponding water) during this time. A comparison of BWE_a estimated from the N_r and measured BWE_a is provided in Figure 8. Periods with overestimation of measured BWE_a corresponded well with the occurrence of strong precipitation events. For instance, the greatest discrepancy with an overestimation of about 4–5 mm occurred at the end of the measurement period during a precipitation event of more than 20 mm/day that may have produced ponding of water at the soil surface. The steep decline in BWE_a in the middle of August is well reflected by the estimated BWE_a obtained from the N_r. To improve the accuracy of the BWE_a prediction, we tested the exclusion of N_r measurements obtained up to 3 days after a 24-hr period with precipitation above 1.5 mm. This data filtering further reduced the RMSE of the BWE_a estimation from 1.3 mm to 0.75 mm (Figure 8, red line).

3.7. Aboveground Dry Biomass Estimation Using the Neutron Ratio

We found that the aboveground dry biomass AGB_d could be estimated from the BWE_a predicted using the N_r with an RMSE of 0.21 kg/m^2 (R^2 = 0.61) when the measured time-variable AGB_r was used (Figure 9). In the case of a static AGB_r, the RMSE increased only slightly to 0.22 kg/m^2 (R^2 = 0.52). Using only the N_r data that were

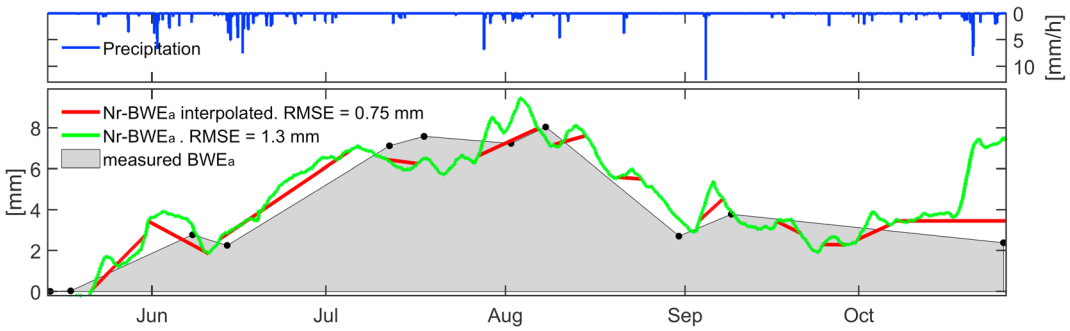

Figure 8. Time series of measured (gray area) and N_r-derived (green) BWE_a. The red line indicates an interpolated time series of N_r-derived BWE_a where data points were removed that occurred within 3 days after a 24-hr period with precipitation ≥1.5 mm. The observed increases in N_r-BWE_a before the respective precipitation events are explained by the use of a 3-day moving average. RMSE = root-mean-square error.

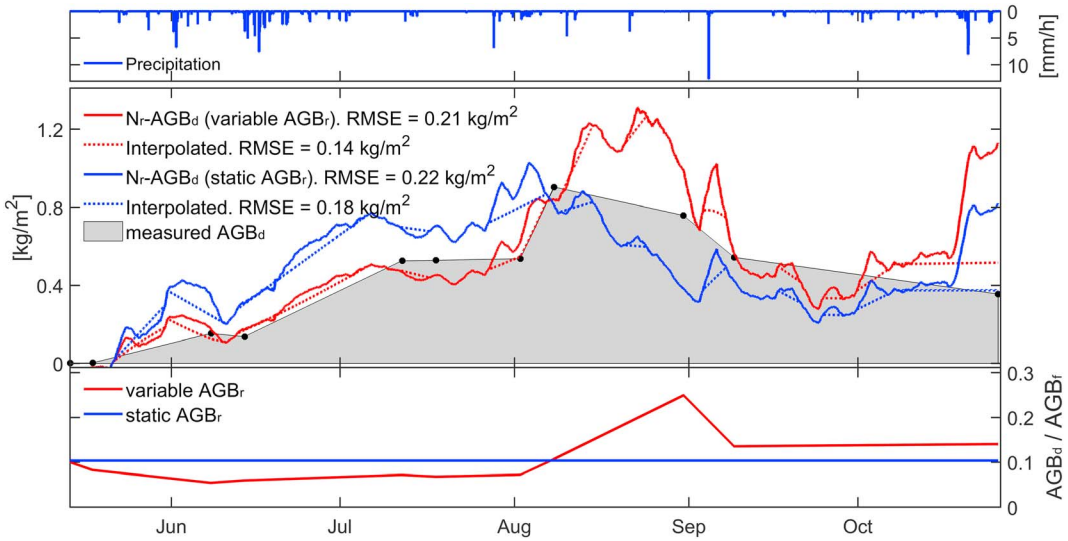

Figure 9. Time series of measured (gray) and N_r-derived dry aboveground biomass ($Nr\text{-}AGB_d$) using a temporally variable (red line) or a mean ratio of dry to fresh biomass (blue line). The dashed lines indicate interpolated time series of $N_r\text{-}AGB_d$ where data points were removed that occurred within 3 days after a 24-hr period with precipitation ≥1.5 mm. The increase in $N_r\text{-}AGB_d$ before precipitation events is explained by the use of a 3-day moving average. RMSE = root-mean-square error.

not affected by precipitation events (i.e., Figure 9, dashed lines), the RMSE improved to 0.14 kg/m^2 (R^2 = 0.92) and 0.18 kg/m^2 (R^2 = 0.67) for the dynamic and static AGB_r, respectively.

The accuracy of the biomass estimates obtained with CRNS compared well with the typical accuracy reported in remote sensing studies. For instance, Bendig et al. (2015) estimated dry aboveground biomass of summer barley based on red-green-blue imaging from an unmanned aerial vehicle with a R^2 of 0.83 and RMSE of 0.35 kg/m^2. Using plant height as an input parameter for a crop model, they achieved a R^2 of 0.85 and a RMSE of 0.324 kg/m^2. Using satellite imagery, Kross et al. (2014) estimated aboveground biomass of soybean and corn with a R^2 of 0.95 and 0.97, respectively.

3.8. SWC Estimation With Biomass Correction Using the Neutron Ratio

We tested whether the combined effect of belowground and aboveground biomass on SWC estimates obtained from CRNS measurements can be corrected using the N_r. For this, in situ measured BWE_b was added to the BWE_a estimated from the N_r (Figure 8, green line) in order to obtain an estimate of BWE_{tot} ($N_r\text{-}BWE_{tot}$ in Figure 10). We found that the use of this $N_r\text{-}BWE_{tot}$ further improved the linear relationship with N_0 as compared to the case with measured BWE_{tot} (R^2 increased from 0.83 to 0.94; cf. Figures 5 [right] and Figure 10). When using this relationship to predict SWC, the RMSE between estimated and reference SWC was further reduced from 0.019 to 0.013 cm^3/cm^3 (Figure 11). Nevertheless, some deviations between predicted and reference SWC are still visible after intensive precipitation events (e.g., beginning of August and September) probably due to effects of ponding of water, intercepted water on leaves, or strong SWC gradients in the soil profile. In comparison to the correction based on measured BWE_{tot}, these deviations were reduced slightly, which may be explained by the implicit inclusion of near-surface water in BWE_a determined from the N_r (Tian et al., 2016).

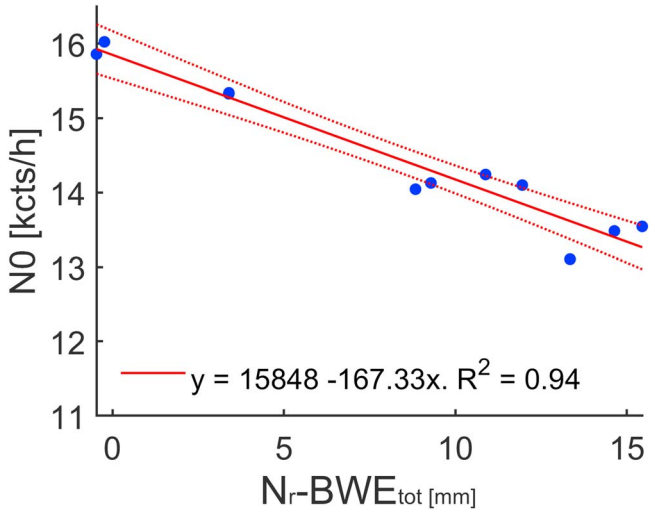

Figure 10. Relationship between N_0 calibrated at the times of biomass measurements using equation (7) and N_r-derived BWE_{tot} (N_r-derived BWE_a as shown in Figure 8 summed with measured BWE_b).

3.9. Relationship Between N_0 and the Neutron Ratio

For the correction of the influence of BWE_a on SWC estimates obtained from CRNS measurements, a calibration between N_0 and BWE_a is not strictly necessary as a regression analysis between N_0

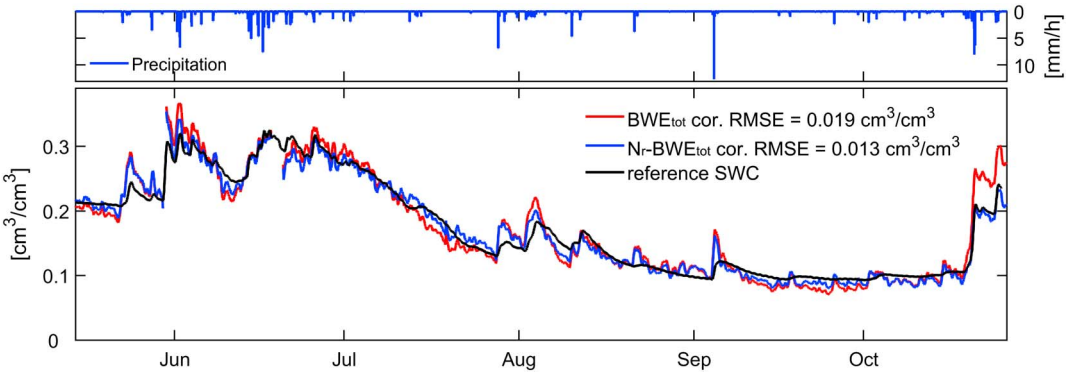

Figure 11. Time series of measured (black line) and *FN*-derived SWC, either corrected using BWE_{tot} (Method 3d, red line) or N_r-derived BWE_{tot} (Method 3e, blue line) using equations (7) and (9). RMSE = root-mean-square error; SWC = soil water content.

(here calibrated for all times with *FN* intensity measurements) and the N_r and the subsequent use of equation (10) would be sufficient (Figure 12). This regression between N_0 and N_r resulted in a relatively low R^2 (0.52) due to additional short-term influences on the N_r (e.g., interception storage and ponding). Nevertheless, a significant linear relationship between N_0 and the N_r was found. From the perspective of correcting CRNS data for dynamic changes in biomass, this approach is far more convenient (i.e., less work intensive and thus less time consuming) than using in situ measurements of BWE_a to correct CRNS data as suggested in other studies (Baatz et al., 2014; Franz, Zreda, Rosolem, & Ferré, 2013; Hawdon et al., 2014; Hornbuckle et al., 2012; Rivera Villarreyes et al., 2011). We found that the use of a linear relationship between N_0 and the N_r was more accurate (RMSE of 0.032 cm^3/cm^3) than the site-specific linear correction model, which yielded a higher RMSE of 0.036 cm^3/cm^3 (Figure 13). This higher accuracy may be explained by a better BWE_a representation of the N_r for the interpolated periods in between biomass samplings and by the implicit consideration of hydrogen stored in additional pools.

4. Discussion

4.1. Comparison of Biomass Correction Methods

In this study, we showed that the simultaneous measurement of aboveground biomass and SWC with CRNS is possible. In addition, it was shown that the accuracy of SWC estimates derived from CRNS measurements improved when variations in aboveground and belowground biomass were considered. We tested several correction methods to account for biomass effects, and the data requirements and the resulting measurement accuracy are summarized in Table 1. As expected from previous studies (e.g., Andreasen, Jensen, Desilets, Zreda, et al., 2017; Baatz et al., 2015), calibration during vegetation-free conditions produced the lowest accuracy (Method 1), as the effect of biomass on the SWC estimates is strongest in this case. Using a time series of in situ SWC estimates for the calibration partly incorporates the effect of biomass in the calibration parameter N_0 (Method 2), and this resulted in periods with systematic underestimation or overestimation of SWC and a relatively high RMSE of 0.046 cm^3/cm^3. This value is the highest accuracy that could be achieved in this study without explicit consideration of the dynamical changes in the size of the hydrogen pool contained in vegetation.

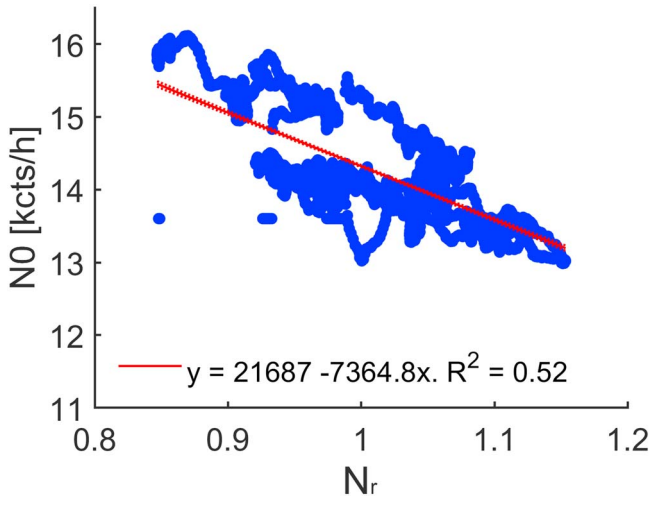

Figure 12. Relationship between N_0 and N_r, where N_0 was determined from the *FN* intensity and the reference soil water content at each measurement time using equation (7) without correction for biomass.

The biomass correction approach of Baatz et al. (2015; Method 3a) was not able to account for the strong biomass effect of the sugar beets in our experiment, as indicated by the high RMSE of 0.095 cm^3/cm^3. A comparison of the linear regression between N_0 and BWE_a based on Baatz et al. (2015) and the site-specific

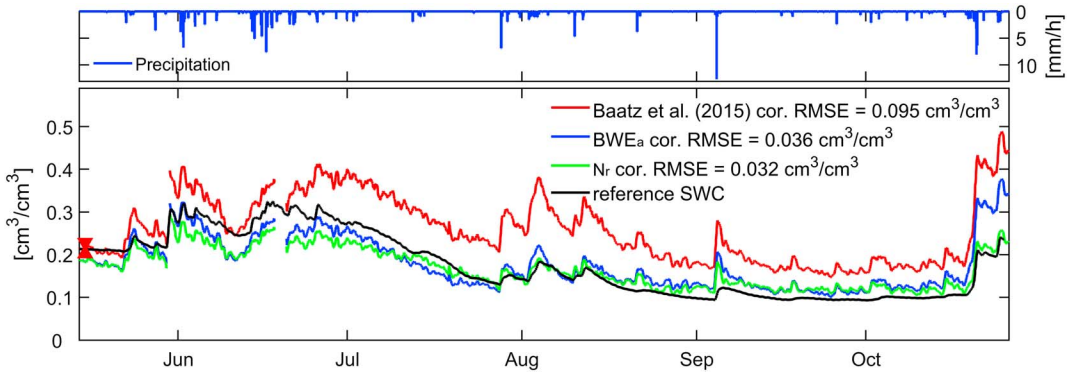

Figure 13. Time series of measured reference SWC (black line), estimated SWC after correction for measured BWE_a using equations (7) and (8) with the site-specific linear regression (Method 3b, blue line; cf. Figure 5, left), estimated SWC calibrated on 15 May (red arrows) and corrected using measured BWE_a with the empirical vegetation correction found by Baatz et al. (2015; Method 3a, red line), and estimated SWC after correction for BWE_a using equations (7) and (10) and the linear relationship between N_r and N_0 (Figure 12, Method 3c, green line). RMSE = root-mean-square error; SWC = soil water content.

measurements (Method 3b) presented in this study (Figure 5, left) shows a strong difference in the slope of the linear relationship (−245 vs. −80). The difference can be explained by the much broader range of aboveground biomass measurements used for their correction function (from bare soil conditions to dense forest sites). This perhaps provides support for the results of Hawdon et al. (2014), who suggested a nonlinear relationship between N_0 and BWE_a with a steep initial decrease of N_0 for low BWE_a and a moderate decrease in N_0 for higher BWE_a. The results also suggest that plant structural properties, such as surface coverage, leaf area index, plant height, and plant phenology, may also influence the relationship between N_0 and BWE. This dependence was already briefly discussed in Franz, Zreda, Rosolem, and Ferré (2013) for forest ecosystems and should be further investigated, for example, using highly resolved neutron transport simulations. The use of both aboveground and belowground biomass measurements for the correction (Methods 3d and 3e) resulted in the highest SWC accuracy (RMSE of 0.19–0.13 cm^3/cm^3), which confirms that the belowground biomass has a strong influence on the FN intensity (e.g., Franz, Zreda, Rosolem, & Ferré, 2013). However, the sampling of roots down to 40 cm is very time consuming and the moderate increase in accuracy of the SWC estimates might not justify this extra work. Alternatively, the use of the N_r for the correction of biomass effects (Methods 3c) considerably improved the accuracy of the SWC measurements by CRNS (RMSE of 0.032 cm^3/cm^3) without the need for biomass determination.

4.2. Potential for Biomass Estimation

The drought conditions in the second half of the measurement period affected the plant development and led to a decrease in aboveground biomass. These conditions provided a good opportunity to test methods to estimate dry aboveground biomass from the N_r, and good accuracy could be achieved (RMSE of 0.14–0.22 kg/m^2). In this context, it is important to realize that satellite-based methods for biomass estimation typically rely on optical methods, which do not represent the drying of leaf biomass well because of the color change from green to yellowish brown (Butterfield & Malmstrom, 2009). Therefore, we expect that biomass estimates from CRNS outperform satellite-based methods in situations with drought-induced biomass decline. This suggests a high potential for the use of CRNS measurements for simultaneous estimation of SWC and biomass, which will be particularly beneficial in semiarid and arid climates.

4.3. Remaining Uncertainties

The remaining uncertainty in the biomass estimates obtained from CRNS measurements was partly associated with precipitation events, which clearly suggests that the N_r is also sensitive to interception, ponding water (Tian et al., 2016), and possibly also to shallow SWC (Andreasen, Jensen, Desilets, Zreda, et al., 2017). Clearly, the accuracy of biomass estimates obtained from CRNS may suffer from these confounding influences in humid or rainy conditions. In an agricultural context, we therefore recommend that the relationship between N_r and N_0 is established using data from periods with dry leaf surfaces and without ponding water.

At the same time, this sensitivity of the N_r to other hydrogen pools also offers opportunities. For example, it may be possible to estimate the interception storage in addition to biomass from the N_r by assuming that these two processes affect the N_r at different time scales, that is, biomass changes occur on weekly time scales whereas interception occurs on daily time scales (Baroni & Oswald, 2015).

Based on their modeling results, Andreasen, Jensen, Desilets, Zreda, et al. (2017) expected that the N_r was independent of SWC, which contradicted their measurement results that clearly showed a relationship between N_r and SWC. In our study, N_r and average SWC at 5-cm depth were uncorrelated ($R^2 = 0.008$). This may partly be explained by the uppermost part of the sugar beets that extruded from the surface (up to ~5 cm) during the later growth stage, which may have attenuated SWC effects on the N_r to some extent. In addition, it has to be noted that SWC variations near the surface (i.e., $<$5 cm below ground) were not captured by our in situ measurements. We also explored whether the N_r can be used to directly predict BWE_b or BWE_{tot}, but no meaningful relationships were found.

In this study, we did not consider that the *FN* and *TN* footprints are likely not the same. This potential scale mismatch may become important in case of strong spatial heterogeneity of soil properties and biomass. However, only the *FN* footprint has been characterized in several modeling studies so far (e.g., Köhli et al., 2015; Schrön et al., 2017; Zreda et al., 2008). The size of the *TN* footprint and the factors that influence it are still unclear and need to be addressed by dedicated neutron modeling studies. Nevertheless, our results indicate that the proposed methods worked well even for a relatively heterogeneous research site (cf. Figure 1).

The results presented in this study are limited to a single vegetation type, and it is likely that the linear relationships reported here cannot be applied to other crops without adjustments in the parameterization. Therefore, further research with different vegetation types is necessary to allow the derivation of more general corrections functions. In particular, it may be possible to relate plant structural properties, such as leaf area index, vegetation height, and the root-to-shoot ratio, to the variables used for the linear regression models.

The experimental setup in this study relied on multiple neutron detectors in order to increase the CRNS sensitivity to the extent possible. It is well established that higher count rates obtained by using more detectors or longer integration times will significantly increase the SWC measurement accuracy as shown by Bogena et al. (2013). Therefore, we recommend using longer integration times for studies that rely on a single detector, and the challenge here is to find a suitable trade-off between count rate uncertainty and time resolution (e.g., 24 hr). For biomass detection using CRNS, our study showed that a 3-day integration time to obtain reliable estimates of N_r is suitable, which is rather long but not problematic due to expected slow changes in biomass. Alternatively, a new generation of detector devices based on boron-10 layers is emerging, which will enable higher count rates at a relatively low price (e.g., Weimar, 2017). Such detectors are expected to open up new possibilities for the detection of hydrogen pools with low residence time (e.g., interception and ponded water).

Finally, it has to be noted that the unshielded neutron detectors used to determine *TN* are also sensitive to *FN* to some extent (5% of the measured neutrons) and that the moderated detectors are also sensitive to *TN* (45% of the measured neutrons; Andreasen et al., 2016; McJannet et al., 2014). Thus, an improved distinction between *TN* and *FN*, for example, using the cadmium difference method developed by Andreasen et al. (2016), would lead to more accurate estimates of the N_r, which may in turn increase the accuracy of the proposed soil moisture and biomass estimation methods.

5. Conclusions and Outlook

In our study with sugar beets, we found that the influence of dynamic changes of aboveground biomass on cosmic ray SWC measurements can be corrected using the ratio of *TN* to *FN* (N_r). This is in agreement with findings of Tian et al. (2016) for other crops (maize and soy bean). We also demonstrated that the N_r approach gives better results compared to the common approach for correcting biomass effects on CRNS data using in situ biomass measurements. Furthermore, we showed that the N_r can also be used for the continuous determination of aboveground BWE and dry aboveground biomass. The impact of dynamic changes in aboveground and belowground BWE could both be considered using linear regressions with the CRNS

calibration parameter N_0. These findings suggest that CRNS measurements can be used for simultaneous measurement of SWC and biomass, for example, to support the investigation of drought effects on crop production.

Future research should aim to confirm the general applicability of the proposed methods for other crops, with a particular focus on crops with less biomass production (e.g., wheat). A particular challenge here is that the N_r is also sensitive to other hydrogen pools located on or close to the soil surface, such as snow, interception, and ponding water. Furthermore, SWC from shallow depth and belowground biomass may also influence the value of the N_r. Thus, future studies should consider monitoring these additional hydrogen pools (e.g., interception storage and ponding water) to allow a better discrimination of the various contributions to the CRNS measurements. However, given the large number of hydrogen pools and the involved measurement challenges, we also suggest using appropriate soil hydrological and vegetation models to support the interpretation of CRNS measurements. Promising choices would be the use of vadose zone models (e.g., HYDRUS-1D; Simunek et al., 2008) that simulate the generation of surface ponding, SWC gradients very close to the soil surface (which is difficult to measure), and water stored in the litter layer (cf. Bogena et al., 2013) or models that simulate soil water and carbon fluxes as well as dynamic plant growth in agricultural systems (e.g., AgroC; Klosterhalfen et al., 2017). The combination with crop growth models is particularly interesting because it would allow to obtain information regarding the root-to-shoot-ratio that relates aboveground and belowground biomass, which is required to estimate belowground biomass from the N_r.

Within the cosmic ray community, mobile measurement systems (i.e., cosmic rovers) are gaining popularity for monitoring SWC of larger areas (Avery et al., 2016; Franz et al., 2015; McJannet et al., 2014). Accurate biomass and SWC data on scales of tens to hundreds of kilometers, which can be provided by cosmic ray roving systems, bear immense potential for resource management. For instance, SWC and dynamic biomass development data can jointly be used as indicators for the control of irrigation systems, with the aim of maximizing the water use efficiency (Jones, 2004). The work presented here extends the use of cosmic rovers to simultaneous measurements of aboveground biomass and SWC and allows the continuous correction of aboveground biomass effects on SWC prediction without the need for laborious local biomass calibration.

Appendix A: In Situ SWC Weighting

The appropriate weights of the in situ SWC sensors depend on the sensing depth of the CRNS probes. In analogy to Franz, Zreda, Rosolem, and Ferré (2012), the sensing depth (D_{86}) is assumed to depend on the soil water equivalent of all hydrogen stored in the soil (θ_{eq}; i.e., SWC + LW + SOW + BWE_b) and is defined as the depth above which 86% of the measured neutrons originate. In addition, D_{86} depends on the distance (r [meters]) between the CRNS probe and the in situ SWC sensors (Köhli et al., 2015). For the weighting of point measurements r is rescaled (r_s) to adapt to pressure and vegetation height variations (Schrön et al., 2017):

$$r_s = r/f_p/f_{veg} \tag{A1}$$

where f_p is the scaling factor for atmospheric pressure and f_{veg} is the scaling factor for vegetation height. They are calculated as follows (Schrön et al., 2017):

$$f_p = \frac{0.5}{0.86 - \exp^{-P/P_{ref}}} \tag{A2}$$

$$f_{veg} = 1 - 0.17 \cdot \left(1 - \exp^{-0.41 \cdot H_{veg}}\right) \cdot \left(1 + \exp^{-9.25 \cdot \theta_{eq,av}}\right) \tag{A3}$$

where P_{ref} is the standard atmospheric pressure at sea level (1,013.25 hPa), P is the measured atmospheric pressure (hPa), H_{veg} is the vegetation height (cm), and $\theta_{eq,\ av}$ is the average soil water equivalent of each SWC measurement profile and given in in cm^3/cm^3, respectively. According to Köhli et al. (2015), a vegetation height of 2 m corresponds to a BWE of 8.8 kg/m^2 in their neutron transport model. We assumed a linear relationship between plant height and aboveground biomass (BWE_a) and used the field measurements of BWE_a to calculate the corresponding H_{veg} values. Then, the penetration depth at each measurement location (D_{86}) can be calculated:

$$D_{86} = \frac{1}{p_{bd}} \cdot \left(p_0 + p_1 \cdot (p_2 + \exp^{-p_3 \cdot r_s}) \cdot \frac{p_4 + \theta_{eq,av}}{p_5 + \theta_{eq,av}} \right) \quad \text{(A4)}$$

where the values of the fitting parameters p_{0-5} are 8.321, 0.14249, 0.96655, 0.01, 20, and 0.0429 (Schrön et al., 2017). The depth-specific weighting factors (W_d) for the in situ SWC sensors and the vertically weighted SWC (θ_{wd}) for the reference SWC stations were calculated using

$$W_d = \exp^{-2d/D_{86}} \quad \text{(A5)}$$

and

$$\theta_{wd} = \frac{\Sigma \theta \cdot W_d}{\Sigma W_d} \quad \text{(A6)}$$

Now, the horizontal weights (W_r) for the SoilNet locations can be calculated using

$$W_r \approx \begin{cases} F_1 \exp^{-F_2 r_s} + F_3 \exp^{-F_4 r_s}; & 1\ \text{m} < r_s \leq 50\ \text{m} \\ F_5 \exp^{-F_6 r_s} + F_7 \exp^{-F_8 r_s}; & 50\ \text{m} < r_s < 600\ \text{m} \end{cases} \quad \text{(A7)}$$

The parametric functions F_{1-8} in equation (A7) consider the local θ_{wd} variations and the influence of atmospheric water content changes. We refer to Schrön et al. (2017) for a full description of the weighting method. They added another parametric function for distances between 0 and 1 m and altered the succeeding parameter functions to be valid from 1 to 50 m. The benefits of the additional parametric function cannot be evaluated in this study, since in situ measurements were only taken at distances larger than 3 m. The final weighted SWC within the CRNS footprint (θ_{hv}) was calculated using

$$\theta_{hv} = \frac{\Sigma \theta_{wd} \cdot W_r}{\Sigma W_r} \quad \text{(A8)}$$

All calculations in Appendix A were iterated until θ_{hv} values converged within 1 vol.% accuracy (Schrön et al., 2017). For this, $\theta_{eq,\ av}$ was substituted with the depth weighted SWC of each measurement profile, θ_{wd} summed with *LW*, *SOW*, and BWE_b.

Appendix B: Neutron Count Corrections

Since the cosmic ray flux through the atmosphere is exponentially attenuated as a function of the traversed cumulative mass, measured neutron count rates need to be normalized to standard atmospheric pressure using

$$N_p = N_{raw} \cdot e^{\left(\frac{P - P_0}{L}\right)} \quad \text{(B1)}$$

where N_p is the neutron count rate corrected for atmospheric pressure, N_{raw} is the raw neutron count rate, P_0 is the reference atmospheric pressure (1,013.25 hPa), P is the actual atmospheric pressure, and L denotes the local mass attenuation length (131.6 g/cm^2; Desilets & Zreda, 2003). The neutron intensity at ground level also strongly depends on the amount of incoming cosmic radiation. In this study, data from neutron monitors at the Jungfraujoch in Switzerland (stations JUNG and JUNG1 averaged, freely available at www.nmdb.eu) were used to correct for incoming radiation using the following correction function:

$$N_{pi} = N_p \cdot \frac{I_{ref}}{I} \quad \text{(B2)}$$

where N_{pi} is the neutron count rate corrected for variations in incoming cosmic radiation, and I and I_{ref} (for this study the mean of I was chosen) are the current and reference neutron monitor count rates, respectively. In a third step, we accounted for the effect of atmospheric water vapor fluctuations on neutron intensity using the approach of Rosolem et al. (2013):

Table C1
RMSE and R^2 (calculated between N_r-derived BWE_a and measured BWE_a) indicating the quality of N_r-based BWE_a estimation using different combinations of TN and FN

RMSE	R^2	TN_{raw}		TN_p		TN_i		TN_h		TN_{pi}		TN_{ph}		TN_{ih}		TN_{pih}	
FN_{raw}		1.9	0.8	1.6	0.8	2.3	0.2	1.8	0.8	2.4	0.5	1.5	0.8	2.3	0.3	2.3	0.5
FN_{pih}		1.8	0.5	1.5	0.9	2.1	0.2	1.7	0.7	2.1	0.8	1.3	1	2.1	0.3	1.9	0.8

Note. The best performing combination with RMSE of 1.3 mm and R^2 of 0.95 is marked in green. RMSE = root-mean-square error.

$$N_{pih} = N_{pi}\cdot\left(1 + 0.0054\cdot\left(p_{v0} - p_{v0}^{ref}\right)\right) \tag{B3}$$

where N_{pih} is the neutron count rate corrected for variations in water vapor, p_{v0} the actual absolute humidity (g/m^3) and p_{v0}^{ref} the reference absolute humidity (0 g/m^3) at 2-m height.

Appendix C: Correction of *TN* Used in the N_r

For our data set, we empirically investigated how *TN* (and *FN*) used for the calculation of the N_r should be corrected to obtain the best estimate of BWE_a with equation (4). The performance was evaluated based on RMSE and R^2. To test the different corrections, we substituted the *TN* and *FN* intensity in equation (3) using combinations of the corrections for pressure (subscript *p*), incoming cosmic radiation (subscript *i*), and atmospheric water vapor (subscript *h*) (see Appendix B). The subscript (raw) indicates the uncorrected neutron intensity measured directly with the cosmic ray probes, which was tested for comparison to Tian et al. (2016). The results are summarized in Table C1. We found the highest R^2 (0.95) and lowest RMSE (1.3 mm) when N_r was calculated from TN_{ph} and FN_{pih}. Therefore, this combination was consequently used for the calculation of the N_r. In the main manuscript, *TN* is used to indicate TN_{ph} and *FN* is used to indicate FN_{pih}.

Appendix D: Derivation of Equation (5)

Here we present the derivation of equation (5) used for the calculation of AGB_d from the N_r. First, we reformulated equation (1) by using AGB_f and AGB_d instead of BM_f and BM_d, respectively:

$$BWE_a = \left[\left(AGB_f - AGB_d\right) + f_{ew}\cdot AGB_d\right]\cdot\rho_w\cdot p_d \tag{D1}$$

Then the combination of equations (D1) and (6) produces equation (D2):

$$BWE_a = \left[\frac{AGB_d}{AGB_r} + AGB_d\cdot f_{ew} - AGB_d\right]\cdot p_w\cdot p_d \tag{D2}$$

Solving for AGB_d, we obtain

$$AGB_d = \frac{BWE_a}{\left(\frac{1}{AGB_r} + f_{ew} - 1\right)}\cdot\frac{1}{p_w\cdot p_d} \tag{D3}$$

Finally, AGB_d and BWE_a where replaced with their N_r-derived counterparts N_r-AGB_d and N_r-BWE_a, respectively.

Acknowledgments
We gratefully acknowledge the support by the SFB-TR32 *Patterns in Soil-Vegetation-Atmosphere Systems: Monitoring, Modelling and Data Assimilation* funded by the Deutsche Forschungsgemeinschaft (DFG) and TERENO (TERrestrial ENvironmental Observatories) funded by the Helmholtz-Gemeinschaft. We also acknowledge the NMDB database funded by EU-FP7. Bernd Schilling, Daniel Dolfus, and Ansgar Weuthen are thanked for support with the installation and maintenance of measurement equipment during the field experiment. Most data presented in this study is freely available via the TERENO data portal (http://teodoor.icg.kfa-juelich.de/ibg3searchportal2/index.jsp).

References

Allen, R. G., Pereira, L. S., Raes, D., & Smith, M. (1998). Crop evapotranspiration—Guidelines for computing crop water requirements. FAO irrigation and drainage paper 56 (15 pp.).

Andreasen, M., Jensen, K. H., Desilets, D., Franz, T., Zreda, M., Bogena, H. R., & Looms, M. C. (2017). Status and perspectives of the cosmic-ray neutron method for soil moisture estimation and other environmental science applications. *Vadose Zone Journal*, *16*(8). https://doi.org/10.2136/vzj2017.04.0086

Andreasen, M., Jensen, K. H., Desilets, D., Zreda, M., Bogena, H. R., & Looms, M. C. (2017). Cosmic-ray neutron transport at a forest field site: Identifying the signature of biomass and canopy interception. *Hydrology and Earth System Sciences*, *21*(4), 1875–1894. https://doi.org/10.5194/hess-21-1875-2017

Andreasen, M., Jensen, K. H., Zreda, M., Desilets, D., Bogena, H. R., & Looms, M. C. (2016). Modeling cosmic-ray neutron field measurements. *Water Resources Research*, *52*, 6451–6471. https://doi.org/10.1002/2015WR018236

Avery, W. A., Finkenbeiner, C., Franz, T. E., Wang, T., Nguy-Robertson, A. L., Suyker, A., et al. (2016). Incorporation of globally available datasets into the roving cosmic-ray neutron probe method for estimating field-scale soil water content. *Hydrology and Earth System Sciences*, *20*(9), 3859–3872. https://doi.org/10.5194/hess-20-3859-2016

Baatz, R., Bogena, H. R., Hendricks Franssen, H.-J., Huisman, J. A., Montzka, C., & Vereecken, H. (2015). An empirical vegetation correction for soil water content quantification using cosmic ray probes. *Water Resources Research*, *51*, 2030–2046. https://doi.org/10.1002/.2014WR016443

Baatz, R., Bogena, H. R., Hendricks Franssen, H.-J., Huisman, J. A., Qu, W., Montzka, C., & Vereecken, H. (2014). Calibration of a catchment scale cosmic-ray probe network: A comparison of three parametrization methods. *Journal of Hydrology*, *516*, 231–244. https://doi.org/10.1016/j.jhydrol.2014.02.026

Baatz, R., Hendricks Franssen, H.-J., Han, X., Hoar, T., Bogena, H. R., & Vereecken, H. (2017). Evaluation of a cosmic-ray neutron sensor network for improved land surface model prediction. *Hydrology and Earth System Sciences*, *21*(5), 2509–2530. https://doi.org/10.5194/hess-21-2509-2017

Baroni, G., & Oswald, S. E. (2015). A scaling approach for the assessment of biomass changes and rainfall interception using cosmic-ray neutron sensing. *Journal of Hydrology*, *525*, 264–276. https://doi.org/10.1016/j.jhydrol.2015.03.053

Bendig, J., Yu, K., Aasen, H., Bolten, A., Bennertz, S., Broscheit, J., et al. (2015). Combining UAV-based plant height from crop surface models, visible, and near infrared vegetation indices for biomass monitoring in barley. *International Journal of Applied Earth Observation and Geoinformation*, *39*, 79–87. https://doi.org/10.1016/j.jag.2015.02.012

Bogena, H., Kunkel, R., Krüger, E., Zacharias, S., Pütz, T., Schwank, M., et al. (2012). TERENO—Long-term monitoring network for terrestrial research. *Hydrologie und Wasserwirtschaft*, *56*, 138–143.

Bogena, H. R., Herbst, M., Huisman, J. A., Rosenbaum, U., Weuthen, A., & Vereecken, H. (2010). Potential of wireless sensor networks for measuring soil water content variability. *Vadose Zone Journal*, *9*(4), 1002–1013. https://doi.org/10.2136/vzj2009.0173

Bogena, H. R., Huisman, J. A., Baatz, R., Hendricks Franssen, H.-J., & Vereecken, H. (2013). Accuracy of the cosmic-ray soil water content probe in humid forest ecosystems: The worst case scenario. *Water Resources Research*, *49*, 5778–5791. https://doi.org/10.1002/wrcr.20463

Bogena, H. R., Huisman, J. A., Hübner, C., Kusche, J., Jonard, F., Vey, S., et al. (2015). Emerging methods for non-invasive sensing of soil moisture dynamics from field to catchment scale: A review. *WIREs Water*, *2*(6), 635–647. https://doi.org/10.1002/wat2.1097

Bogena, H. R., Huisman, J. A., Schilling, B., Weuthen, A., & Vereecken, H. (2017). Effective calibration of low-cost soil water content sensors. *Sensors*, *17*(12), 208. https://doi.org/10.3390/s17010208

Bogena, H. R., Montzka, C., Huisman, J. A., Graf, A., Schmidt, M., Stockinger, M., et al. (2018). The Rur hydrological observatory: A multi-scale multi-compartment research platform for the advancement of hydrological science. *Vadose Zone Journal*, *17*(1), 1–22. https://doi.org/10.2136/vzj2018.03.0055

Briffa, K. R., van der Schrier, G., & Jones, P. D. (2009). Wet and dry summer in Europe since 1750: Evidence of increasing drought. *International Journal of Climatology*, *29*(13), 1894–1905. https://doi.org/10.1002/joc.1836

Butterfield, H. S., & Malmstrom, C. M. (2009). The effects of phenology on indirect measures of aboveground biomass in annual grasses. *International Journal of Remote Sensing*, *30*(12), 3133–3146. https://doi.org/10.1080/01431160802558774

Dai, A. (2011). Drought under global warming: A review. *Wiley Interdisciplinary Reviews: Climate Change*, *2*, 45–65. https://doi.org/10.1002/wcc.81

Desilets, D., & Zreda, M. (2001). On scaling cosmogenic nuclide production rates for altitude and latitude using cosmic-ray measurements. *Earth and Planetary Science Letters*, *193*(1-2), 213–225. https://doi.org/10.1016/S0012-821X(01)00477-0

Desilets, D., & Zreda, M. (2003). Spatial and temporal distribution of secondary cosmic-ray nucleon intensities and applications to in situ cosmogenic dating. *Earth and Planetary Science Letters*, *206*(1-2), 21–42. https://doi.org/10.1016/S0012-821X(02)01088-9

Desilets, D., Zreda, M., & Ferré, T. P. A. (2010). Nature's neutron probe: Land surface hydrology at an elusive scale with cosmic rays. *Water Resources Research*, *46*, W11505. https://doi.org/10.1029/2009WR008726

Franz, T. E., Wang, T., Avery, W., Finkenbiner, C., & Brocca, L. (2015). Combined analysis of soil moisture measurements from roving and fixed cosmic ray neutron probes for multiscale real-time monitoring. *Geophysical Research Letters*, *42*, 3389–3396. https://doi.org/10.1002/2015GL063963

Franz, T. E., Zreda, M., Ferré, T. P. A., Rosolem, R., Zweck, C., Stillman, S., et al. (2012). Measurement depth of the cosmic-ray soil moisture probe affected by hydrogen from various sources. *Water Resources Research*, 48, W08515. https://doi.org/10.1029/2012WR011871

Franz, T. E., Zreda, M., Rosolem, R., & Ferré, T. P. A. (2012). Field validation of a cosmic-ray neutron sensor using a distributed sensor network. *Vadose Zone Journal*, *11*(4), 11. https://doi.org/10.2136/vzj2012.0046

Franz, T. E., Zreda, M., Rosolem, R., & Ferré, T. P. A. (2013). A universal calibration function for determination of soil moisture with cosmic-ray neutrons. *Hydrology and Earth System Sciences*, *17*(2), 453–460. https://doi.org/10.5194/hess-17-453-2013

Franz, T. E., Zreda, M., Rosolem, R., Hornbuckle, B. K., Irvin, S. L., Adams, H., et al. (2013). Ecosystem-scale measurements of biomass water using cosmic ray neutrons. *Geophysical Research Letters*, *40*, 3929–3933. https://doi.org/10.1002/grl.50791

Gebler, S., Hendricks Franssen, H.-J., Pütz, T., Post, H., Schmidt, M., & Vereecken, H. (2015). Actual evapotranspiration and precipitation measured by lysimeters: A comparison with eddy covariance and tipping bucket. *Hydrology and Earth System Sciences*, *19*(5), 2145–2161. https://doi.org/10.5194/hess-19-2145-2015

Hawdon, A., McJannet, D., & Wallace, J. (2014). Calibration and correction procedures for cosmic-ray neutron soil moisture probes located across Australia. *Water Resources Research*, *50*, 5029–5043. https://doi.org/10.1002/2013WR015138

Heidbüchel, I., Güntner, A., & Blume, T. (2016). Use of cosmic-ray neutron sensors for soil moisture monitoring in forests. *Hydrology and Earth System Sciences*, *20*(3), 1269–1288. https://doi.org/10.5194/hess-20-1269-2016

Hornbuckle, B., Irvin, S., Franz, T., Rosolem, R., & Zweck, C. (2012). The potential of the COSMOS network to be a source of new soil moisture information for SMOS and SMAP. Geoscience and Remote Sensing Symposium (IGRASS). *IEEE International*, 1243–1246. https://doi.org/10.1109/IGARSS.2012.6351317

Jones, H. G. (2004). Irrigation scheduling: Advantages and pitfalls of plant-based methods. *Journal of Experimental Botany*, *55*(407), 2427–2436. https://doi.org/10.1093/jxb/erh213

Kędzior, M., & Zawadzki, J. (2016). Comparative study of soil moisture estimations from SMOS satellite mission, GLDAS database, and cosmic-ray neutrons measurements at COSMOS station in eastern Poland. *Geoderma*, *283*, 21–31. https://doi.org/10.1016/j.geoderma.2016.07.023

Klosterhalfen, A., Herbst, M., Weihermüller, L., Graf, A., Schmidt, M., Stadler, A., et al. (2017). Multi-site calibration and validation of a net ecosystem carbon exchange model for croplands. *Ecological Modelling*, *363*, 137–156. https://doi.org/10.1016/j.ecolmodel.2017.07.028

Köhli, M., Schrön, M., Zreda, M., Schmidt, U., Dietrich, P., & Zacharias, S. (2015). Footprint characteristics revised for field-scale soil moisture monitoring with cosmic-ray neutrons. *Water Resources Research*, *51*, 5772–5790. https://doi.org/10.1002/2015WR017169

Korres, W., Reichenau, T. G., Fiener, P., Koyama, C. N., Bogena, H. R., Cornelissen, T., et al. (2015). Spatio-temporal soil moisture patterns—A meta-analysis using plot to catchment scale data. *Journal of Hydrology*, *520*, 326–341. https://doi.org/10.1016/j.jhydrol.2014.11.042

Kross, A., McNairn, H., Lapen, D., Sunohara, M., & Champage, C. (2014). Assessment of RapidEye vegetation indices for estimation of leaf area index and biomass in corn and soybean crops. *International Journal of Applied Earth Observation and Geoinformation*, *34*, 235–248. https://doi.org/10.1016/j.jag.2014.08.002

McJannet, D., Franz, T., Hawdon, A., Boadle, D., Baker, B., Almeida, A., et al. (2014). Field testing of the universal calibration function for determination of soil moisture with cosmic-ray neutrons. *Water Resources Research*, *50*, 5235–5248. https://doi.org/10.1002/2014WR015513

Montzka, C., Bogena, H. R., Zreda, M., Monerris, A., Morrison, R., Muddu, S., & Vereecken, H. (2017). Validation of spaceborne and modelled surface soil moisture products with cosmic-ray neutron probes. *Remote Sensing*, *9*(2), 103. https://doi.org/10.3390/rs9020103

Narasimhan, B., & Srinivasan, R. (2005). Development and evaluation of soil moisture deficit index (SMDI) and evapotranspiration deficit index (ETDI) for agricultural drought monitoring. *Agricultural and Forest Meteorology*, *133*(1-4), 69–88. https://doi.org/10.1016/j.agrformet.2005.07.012

Passioura, J. B., & Angus, J. F. (2010). Improving productivity of crops in water-limited environments. *Advances in Agronomy*, *106*, 37–75. https://doi.org/10.1016/S0065-2113(10)06002-5

Rivera Villarreyes, C. A., Baroni, G., & Oswald, S. E. (2011). Integral quantification of seasonal soil moisture changes in farmland by cosmic-ray neurons. *Hydrology and Earth System Sciences*, *15*(12), 3843–3859. https://doi.org/10.5194/hess-15-3843-2011

Rosolem, R., Shuttleworth, W. J., Zreda, M., Franz, T. E., Zeng, X., & Kurc, S. A. (2013). The effect of atmospheric water vapor on the cosmic-ray soil moisture signal. *Journal of Hydrometeorology*, *14*(5), 1659–1671. https://doi.org/10.1175/JHM-D-12-0120.1

Rudolph, S., van der Kruk, J., von Hebel, C., Ali, M., Herbst, M., Montzka, C., et al. (2015). Linking satellite derived LAI patterns with subsoil heterogeneity using large-scale ground-based electromagnetic induction measurements. *Geoderma*, *241-242*, 262–271. https://doi.org/10.1016/j.geoderma.2014.11.015

Schattan, P., Baroni, G., Oswald, S. E., Schober, J., Fey, C., Kormann, C., et al. (2017). Continuous monitoring of snowpack dynamics in alpine terrain by aboveground neutron sensing. *Water Resources Research*, *53*, 3615–3634. https://doi.org/10.1002/2016WR020234

Schrön, M. (2017). Cosmic-ray neutron sensing and its applications to soil and land surface hydrology—On neutron physics, method development, and soil moisture estimation across scales (PhD dissertation, pp. 224). University of Potsdam.

Schrön, M., Köhli, M., Scheiffele, L., Iwema, J., Bogena, H. R., Lv, L., et al. (2017). Improving calibration and validation of cosmic-ray neutron sensors in the light of spatial sensitivity—Theory and evidence. *Hydrology and Earth System Sciences*, *21*(10), 5009–5030. https://doi.org/10.5194/hess-21-5009-2017

Simunek, J., van Genuchten, M. T., & Sejna, M. (2008). Development and applications of the HYDRUS and STANMOD software packages and related codes. *Vadose Zone Journal*, *7*(2), 587–600. https://doi.org/10.2136/vzj2007.0077

Tian, Z. C., Li, Z. Z., Liu, G., Li, B. G., & Ren, T. S. (2016). Soil water content determination with cosmic-ray neutron sensor: Correcting aboveground hydrogen effects with thermal/fast neutron ratio. *Journal of Hydrology*, *540*, 923–933. https://doi.org/10.1016/j.jhydrol.2016.07.004

Topp, G. C., Davis, J. L., & Annan, A. P. (1980). Electromagnetic determination of soil water content: Measurements in coaxial transmission lines. *Water Resources Research*, *16*(3), 574–582. https://doi.org/10.1029/WR016i003p00574

Vereecken, H., Huisman, J. A., Hendricks Franssen, H.-J., Brüggemann, N., Bogena, H. R., Kollet, S., et al. (2015). Soil hydrology: Recent methodological advances, challenges, and perspectives. *Water Resources Research*, *51*, 2616–2633. https://doi.org/10.1002/2014WR016852

Vinodkumar, I. D., Bally, J., Steinle, P., McJannet, D., & Walker, J. (2017). Comparison of soil wetness from multiple models over Australia with observations. *Water Resources Research*, *53*, 633–646. https://doi.org/10.1002/2015WR017738

Webber, H., Gaiser, T., & Ewert, F. (2014). What role can crop models play in supporting climate change adaptation to enhance food security in sub-Saharan Africa? *Agricultural Systems*, *127*, 161–177. https://doi.org/10.1016/j.agsy.2013.12.006

Weihermüller, L., Huisman, J. A., Lambot, S., Herbst, M., & Vereecken, H. (2007). Mapping the spatial variation of soil water content at the field scale with different ground penetrating radar techniques. *Journal of Hydrology*, *340*(3-4), 205–216. https://doi.org/10.1016/j.jhydrol.2007.04.013

Weimar, J. (2017). Entwicklung und Charakterisierung eines 10B-basierten Neutronendetektionssystem zur Bestimmung von Bodenfeuchte auf Hektarskala (MA thesis, pp. 89). University of Heidelberg.

Zacharias, S., Bogena, H. R., Samaniego, L., Mauder, M., Fuss, R., Puetz, T., et al. (2011). A network of terrestrial environmental observatories in Germany. *Vadose Zone Journal*, *10*(3), 955–973. https://doi.org/10.2136/vzj2010.0139

Zink, M., Samaniego, L., Kumar, R., Thober, S., Mai, J., Schäfer, D., & Marx, A. (2016). The German drought monitor. *Environmental Research Letters*, *11*(7). https://doi.org/10.1088/1748-9326/11/7/074002

Zreda, M., Desilets, D., Ferré, T. P. A., & Scott, R. L. (2008). Measuring soil moisture content non-invasively at intermediate spatial scale using cosmic-ray neutrons. *Geophysical Research Letters*, *35*, L21402. https://doi.org/10.1029/2008GL035655

Zreda, M., Shuttleworth, W. J., Xeng, X., Zweck, C., Desilets, D., Franz, T. E., et al. (2012). COSMOS: The COsmic-ray Soil Moisture Observing System. *Hydrology and Earth System Sciences*, *16*(1), 1–18. https://doi.org/10.5194/hess-16-1-2012